JOURNAL OF MATERIALS SCIENCE 32 (1997) 1555–1562

Effect of grain boundary orientation on the sensitization of austenitic stainless steel

A. KAVNER, T. M. DEVINE
Department of Materials Science and Mineral Engineering, University of California, Berkeley, CA 94720, USA

The effect of grain misorientation on the sensitization of grain boundaries in austenitic stainless steel was investigated by sensitizing samples consisting of a large number of 50–80 μm size grains that were sintered to flat, 10 mm^2 single crystals. Seven different sensitization treatments were employed and samples were intergranulary corroded in the modified Strauss test. X-ray pole figures were obtained for each sample and were used to identify the grain misorientations that were resistant to sensitization. In general, macroscopic grain boundary geometry could not explain the sensitization behaviour of most grain boundaries. Nevertheless, the $\Sigma = 9$ boundary was found to be especially resistant to sensitization. Results suggest that grain misorientation primarily affects the growth of sensitization rather than its nucleation. Finally, the crystallographic plane of the grain boundary appears to have an effect on sensitization.

1. Introduction

Electrochemical and electron-probe studies of sensitized stainless steels have shown that the extent of intergranular corrosion is not the same on all grain boundaries. Transmission electron microscopy (TEM) results show that some grain boundaries within a sample may exhibit extensive carbide percipitation, while other boundaries show discontinuous precipitation, or even no carbides at all [1–3]. Presumably, this non-homogeneous precipitation is a consequence, at least in part, of the structures of the grain boundaries.

A complete macroscopic description of a grain boundary includes nine parameters: three degrees of freedom for each grain, and a final three describing the plane boundary separating the two grains [4]. To aid in picturing grain boundary phenomena, it is sometimes preferable to have a microscopic description of the boundary; a way to specify idealized atomic positions in the grain boundary. Specific misorientation between adjacent grains are readily characterized by the coincident site lattice (CSL) model [5]. For certain misorientations a significant fraction, Σ^{-1} of the lattice sites in one grain coincide with the lattice sites in the adjacent grain. These boundaries are denoted "special" by the CSL model. In this model, a boundary is described only by defining the orientation of one grain with respect to the other in terms of an angle-axis pair. The information about the plane adjoining the two grains is lost. Even so, some special high-angle grain boundaries (low Σ^{-1}) are observed to exhibit "special" properties such as low energy and resistance to solute segregation. It is possible that such grain boundaries may also be resistant to sensitization.

Recent work by Liu *et al.* [6] on a nickel-based ternary alloy (Ni–18Cr–18Fe), has supported this idea. They showed that increasing the special grain boundary ($\Sigma \leq 29$) frequency in the thermomechanically processed Alloy 600 from 37 to 72% resulted in commensurate decreases in bulk intergranular corrosion susceptibility in both solution annealed and sensitized conditions. However, earlier work by Ortner and Randle [7] suggested that misorientation alone was not adequate to explain the susceptibility/resistance of a grain boundary to sensitization. The authors stated that the boundary plane, lost in the CSL description of grain misorientation, must be considered. This is consistent with the fact that CSL boundaries with low Σ do not all exhibit special properties. For example, Laws and Goodhew [8] measured the chromium concentration profiles perpendicular to the grain boundary for 50 different boundaries in a sensitized heat treated 316 stainless steel. Some boundaries with $\Sigma = 3$, 11, 13a and 13b exhibited very narrow chromium depleted zones while other boundaries with $\Sigma = 9$ exhibited wide chromium depleted zones. The authors used the structural units model [9], another microscopic description, where a grain boundary is described in terms of a two-dimensional array of specific polyhedral units. Specifically, boundaries with narrow chromium-depleted zones were thought to be "favoured" grain boundaries, which consist of a single type of structural unit, while grain boundaries with wide chromium-depleted zones were thought to be "non-favoured" grain boundaries, which consist of mixtures of several structural units.

In summary, it appears that the resistance of a grain boundary to sensitization may be related, at least in part, to the orientation relationship between the adjacent grains. The validity of this statement is further explored in the present investigation by observing the

0022–2461

sensitization behaviour of a large number of grain boundaries.

The difficulty in earlier attempts to characterize the influence of grain orientations on sensitization is that the techniques of measurement that were employed required the use of sophisticated and expensive equipment, such as transmission electron microscopes, and were generally time-consuming so that information was only obtained on a relatively small number of grain boundaries. In the present study a technique is employed that enables the measurement of the misorientation of a large number of grain boundaries and permits the investigation of grain orientation on the susceptibility of an alloy to sensitization.

The technique originates from a suggestion made by Shewmon [10] that preferential orientations of adjacent grains could be measured by bringing single crystal balls into contact at high temperatures and allowing them to align themselves into the lowest energy configuration. Herrmann *et al.* [11] used this approach in determining the lowest energy orientations of copper by placing a large number of spherical powder particles onto the flat surface of a single crystal of copper. The assembly was then heat treated and the orientations of the powder particles were then determined by X-ray diffraction.

In the present study we were interested not in rotation, but in how grain boundary orientation determines the degree of sensitization. Consequently, we borrowed Herrmann *et al.*'s method [11] to prepare samples with a large number of randomly oriented grain boundaries. Instead of using spherical powder particles which could rotate relatively quickly into low energy orientations, we used tiny, individual grains extracted from a polycrystal of 304 stainless steel.

The individual grains were then placed on top of the flat surface of a single crystal and sintered. The relatively short sintering time and faceted grain morphology ensured a large number of variously oriented grain boundaries. The samples were sensitized and immersed in an aqueous solution of acidified copper sulfate in order to corrode the sensitized grain boundaries. Grains whose boundaries were intergranularly corroded fell off the sample. The grains left on the sample were not susceptible to intergranular corrosion and their orientations and that of the single crystal base plate were measured by X-ray diffraction.

2. Experimental procedure

2.1. Preparation of large grained austenite plates

Large grains in the austenite baseplate were prepared by a recrystallization and grain growth process. 1.5 cm × 1 cm × 0.1 cm plates of austenitic stainless steel of the composition shown in Table I were cold-rolled 2–5%, cleansed, wrapped in tantalum foil, and encapsulated in an argon atmosphere in quartz. The samples were given a grain-growth heat-treatment of 96 h at 1250 °C. The largest grains were about 10 mm^2 and most grains were twinned. The largest grain within each baseplate crystal was marked by an engraver to ensure that it would be centred on the X-ray apparatus. A pole figure was obtained from each single crystal to determine the orientation of the crystal with respect to the plane of the plate.

TABLE I Austenitic stainless steel composition (wt %)

Cr	Ni	C	Mn	Si	S + P
18	12	0.06	1.5	1.5	0.025

2.2. Preparation of individual austenite grains

The austenite grains were prepared from polycrystalline austenite using a sensitization process. Austenite plates of the composition shown in Table I were cleansed, wrapped in tantalum foil, then encapsulated in Pyrex under an argon atmosphere. The samples were given a severe sensitizing heat treatment of 600 °C for 48 h and quenched in ice water. The samples were abraded to remove any oxidized layer caused by the quench, and again ultrasonically cleansed in detergent and distilled water. Copper turnings were wrapped around each sample, and the sample was immersed in boiling, acidified copper sulfate solution according to ASTM-A262E specifications [12]. The samples, disintegrating from the corrosion treatment, were removed from the solution and dipped into concentrated nitric acid which dissolved away any copper remnant while leaving the steel intact. The samples, now a set of crumbly grains, were immersed in a glass beaker of distilled water that was placed in an ultrasonic cleaner. The ultrasonic vibrations separated the sample into individual grains. The grains were dried and sorted by grain size in an ultrasonic sieve. About two cubic centimetres of the grains between 58 and 88 μm were collected.

2.3. Sinter treatment

The 55–88 μm single crystal austenite grains were sifted to form a single layer on each large grained austenite plate and given a sintering treatment of 1250 °C for one hour under a reducing atmosphere of flowing hydrogen. The samples were removed from the furnace, water-quenched, and examined by scanning electron microscopy (SEM).

2.4. Sensitization treatments

The sintered samples were then ultrasonically cleaned in detergent and distilled water, and dried and wrapped in tantalum foil. All samples were encapsulated in Pyrex sealed off under 1.7×10^4 Pa argon. Isothermal sensitization treatments took place in a triple zone furnace; all samples were water quenched upon removal from the furnace. The six sensitization samples were treated at 550 °C for 30 min, 1 and 8 h; and at 600 °C for 30 min, 1 and 8 h. Three samples were given low temperature sensitization treatments in a two-part process. All three samples were given a nucleation treatment at 700 °C for 30 min. Two of the samples

were then re-cleansed, wrapped in fresh tantalum foil, and encapsulated in separate Pyrex tubes in an argon atmosphere for the low temperature sensitization treatments. The samples were treated at 475 °C for 24 and 48 h. The third sample was not given a low temperature treatment after the original nucleation treatment.

All samples were covered with copper shot and immersed in boiling acidified copper sulfate solution, according to ASTM-A262E standards [12]. The samples were removed after 72 h and ultrasonically cleaned for 5 min. This cleansing treatment also served to remove any of the powder that had been sensitized by the treatment and intergranulary corroded. A pole figure was taken of the sample consisting of the plate plus any powder whose boundary with the plate had remained unsensitized.

2.5. X-ray texture analysis

All X-ray work was performed on the Huber pole figure goniometer in the texture laboratory of the Department of Geology and Geophysics, University of California, Berkeley. All pole figures were performed using monochromatic FeK_α at 40 kV accelerating voltage, 10 mA current, with a count time of 10 s. The incoming X-ray beam was collimated so that the diameter was 1 mm. The X-ray peak corresponding to austenite 1 1 1 was located by a 2θ scan on a polycrystalline austenite sample. Then the collimated beam was centred within the large baseplate crystal. The value of θ was kept constant at the austenite (1 1 1) peak while χ and φ were varied by five degree increments, resulting in plots of (1 1 1) intensities on a $5^\circ \times 5^\circ$ equal angle stereographic projection. The program corrected for background by subtracting the background noise level at each χ. The data was collected by the local TEXGON2 program with a personal computer, and existing software programs, POD and PFCONT, were used to calculate and print out the pole figures on stereographic projections.

2.6. Sample analysis

The data were printed as pole figures on 9 cm radius stereographic projections. At least two poles from the baseplate were needed to determine its orientation unambiguously. A Wulff net was used to measure angles between the single crystal austenite poles and the poles corresponding to the sintered powder. A detailed explanation of the data analysis is provided elsewhere [13]. One of the samples was also examined both before and after the sensitization treatment and corrosion test using a scanning electron microscope.

3. Results

Fig. 1 is a scanning electron micrograph showing the density of grains sintered onto a large grain (single crystal) in the baseplate. A single layer of uniformly sized grains covers approximately 60% of the surface area of the plate. Fig. 2 shows a scanning electron micrograph of the sintered interface between baseplate and grain and reveals a grooved neck region, which was a characteristic of all the sintered regions.

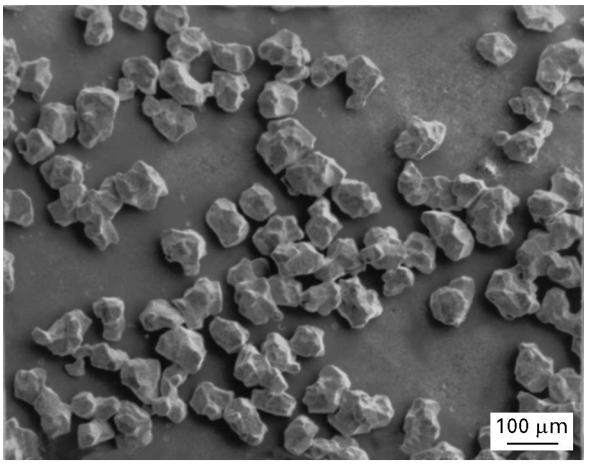

Figure 1 Scanning electron micrograph of sample consisting of large, single crystal baseplate of austenite and a large number of smaller grains, which have been sintered to the baseplate.

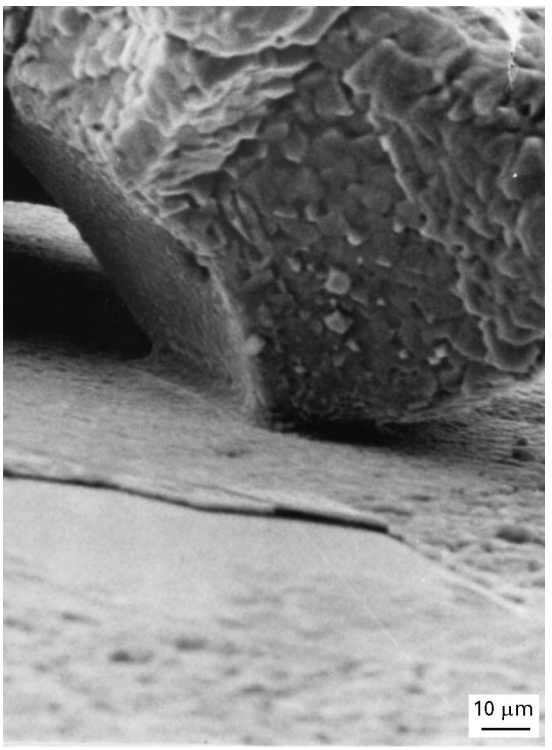

Figure 2 Scanning electron micrograph illustrating the sintered region of the sample.

Fig. 3 shows a scanning electron micrograph of the sample after it had been sensitized for 8 h at 550 °C and corroded in the ASTM-A262E test. Much of the powder has been corroded away, and the structure of the surface appears smoother where the grain had fallen off. A closer look at the smoother patches and details of the pitting of the surface are revealed in Fig. 4. The smoother patches are of two types: one type is a tufted surface which has a small tuft or ridge down the centre, and the other type of surface is smooth. The interface between the baseplate and the powder appears planar in the smooth surface, and planar except for the ridge in the tufted surface.

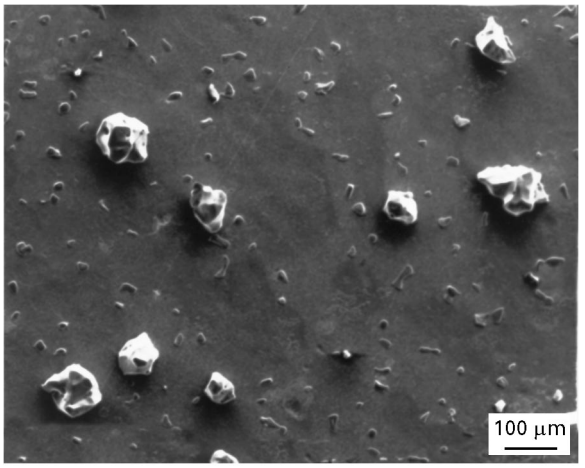

Figure 3 Scanning electron micrograph illustrating the appearance of the sintered sample following sensitizing treatment and 24 h of immersion in ASTM-A262E.

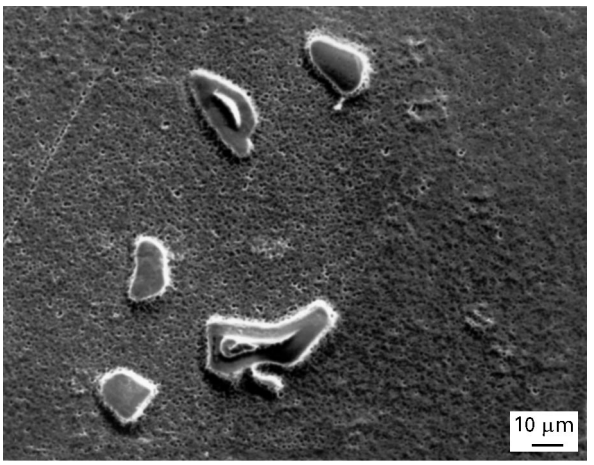

Figure 4 Scanning electron micrograph of the sintered interfaces formed with grains that have failed by intergranular corrosion.

The results from the X-ray pole figure experiments are summarized in the first three columns of Table II. In all, approximately 1000 individual grains were initially attached to the seven single crystals. Following sensitizing heat treatments and corrosion testing, a total of 48 grains remained attached to the baseplates. Obviously, the fraction of sensitization-resistant grain boundaries was very low.

4. Discussion

4.1. Sintered grain structure

The SEM micrographs of the former area of contact between the sintered grain and plate indicate that the grain boundary surface was approximately planar and parallel to the surface of the baseplate. Hence, once the orientation of both the baseplate and a particle are known, the grain boundary orientation is defined macroscopically. It is also interesting to note that the grain boundary surfaces moved from the original interface between the particle and the baseplate and into the particle. This can be seen in Fig. 2 and is similar to observations made by Herrmann *et al.* [11] on spherical powder particles sintered to a flat plate. The grain boundary migrates to the position of minimum surface area.

The tufted features visible on the corroded grain boundaries in Fig. 4 are patches of the grain boundary which failed by ductile fracture following corrosion testing in the A262E test. The presence of the ductile fracture features surrounded by a smoother area of former boundary contact indicates that some grain boundaries were partially corroded and then dropped off by mechanical fracture, presumably occurring during handling of the sample. This points out one limitation of this technique is studying sensitization. Some grains with partially corroded boundaries may remain attached to the baseplate while others may fracture mechanically and fall off. Consequently, the results of this test could be ambiguous for grain boundaries with intermediate degrees of sensitization. Nevertheless, it is clear that severely sensitized grain boundaries are corroded and that the surviving grains formed boundaries that were resistant to sensitization. It is noteworthy that the small amount of powder that survived the sensitization tests does not hamper the ability to measure the powder/baseplate orientation relationship, because the grain sample volume is large enough for the X-ray apparatus to measure the orientation of a single particle of powder.

The powder particles remaining after the A262E test [12] are the result of special sensitization-resistant powder/baseplate orientations. A boundary could be resistant to sensitization for many reasons [14, 15]. The boundary could be such that carbides were not nucleated, or could not grow quickly enough. Or, sensitization was prevented by fast chromium diffusion to that boundary so a depleted zone was quickly replenished. In addition, perhaps insufficient chromium diffusion occurred so that the minimum width required for sensitization could not be reached or the carbide spacing was too large to provide a continuous intergranular path of chromium depletion. The composition of the alloy studied, specifically its chromium and carbon contents, the heat treatments employed, and the fact that the vast majority of the grain boundaries were severely sensitized suggests that replenishment of chromium-depleted zones is not a likely explanation for the sensitization resistance of the grain boundaries formed by the grains listed in Table II. However, it is not possible at this juncture to distinguish among the three other possible causes for sensitization resistance.

4.2. Geometric interpretation of orientation results

The orientation data from the small percentage of grains that remained unsensitized is listed as axis-angle pairs in column 4 of Table II. The purpose of the present study was to determine the orientation relationship between these remaining grains and the single crystal baseplate. The results presented in Table II indicate that a number of these boundaries were special grain boundaries determined by the CSL model. These are shown in the fifth column of the table. The deviation from exact CSL misorientation is

TABLE II Results of X-ray pole figure analyses of sensitized and intergranularly corroded samples

Heat treatment	Plane of baseplate	Orientation relationship between baseplate and powder	Angle-axis pair	CSL correlation	Angle deviation < Brandon criterion
550 °C/0.5 h	(8 1 8)	$(1\,1\,1)_{powder}\|(5\,1\,1)_{plate}$	[1 2 3], 56.25°	⟨3 2 1⟩ 123.75° Σ = 9	0.00°
550 °C/0.5 h	(8 1 8)	$(1\,1\,1)_{powder}\|(7\,7\,\underline{2})_{plate}$	[1 1 0], 46.69°	⟨1 1 0⟩ 50.48° Σ = 11	3.79° < 4.52°
550 °C/0.5 h	(8 1 8)	$(1\,1\,1)_{powder}\|(1\,3\,4)_{plate}$	[1 3 2], 22.5°	None	
550 °C/1 h	(3 1 8)	$(1\,1\,1)_{powder}\|(1\,2\,1)_{plate}$	[1 0 1], 19.47°	None	
550 °C/1 h	(3 1 8)	$(1\,1\,1)_{powder}\|(\underline{1}\,1\,3)_{plate}$	[1 2 1], 58.52°	⟨2 1 1⟩ 135.58° Σ = 7	5.19° < 5.67°
550 °C/1 h	(3 1 8)	$(1\,1\,1)_{powder}\|(\underline{1}\,\underline{1}\,7)_{plate}$	[1 1 0], 66.16°	⟨1 1 0⟩ 70.53° Σ = 3	6.09° < 8.66°
550 °C/1 h	(3 1 8)	$(1\,1\,1)_{powder}\|(1\,\underline{1}\,4)_{plate}$	[5 3 2], 74.21°	None	
550 °C/1 h	(3 1 8)	$(1\,1\,1)_{powder}\|(\underline{1}\,\underline{2}\,5)_{plate}$	[7 6 1], 77.83°	None	
550 °C/1 h	(3 1 8)	$(1\,1\,1)_{powder}\|(\underline{2}\,\underline{3}\,5)_{plate}$	[8 7 1], 90°	⟨3 2 1⟩ 123.75° Σ = 9	4.77 < 5.67
550 °C/1 h	(3 1 8)	$(1\,1\,1)_{powder}\|(1\,\underline{4}\,8)_{plate}$	[4 7 5], 71.29°	None	
550 °C/1 h	(3 1 8)	$(1\,1\,1)_{powder}\|(1\,1\,2)_{plate}$	[1 1 0], 19.47°	⟨1 1 0⟩ 50.48° Σ = 11	4.26° < 4.25°
550 °C/1 h	(3 1 8)	$(1\,1\,1)_{powder}\|(4\,3\,0)_{plate}$	[3 4 1], 36.07°	None	
550 °C/1 h	(3 1 8)	$(1\,1\,1)_{powder}\|(7\,3\,6)_{plate}$	[3 1 4], 17.68°	⟨1 1 0⟩ 70.53° Σ = 3	4.26° < 8.66°
550 °C/1 h	(3 1 8)	$(1\,1\,1)_{powder}\|(3\,1\,4)_{plate}$	[3 1 2], 59.53°	None	
550 °C/1 h	(3 1 8)	$(1\,1\,1)_{powder}\|(1\,0\,2)_{plate}$	[2 1 1], 39.23°	None	
550 °C/1 h	(3 1 8)	$(1\,1\,1)_{powder}\|(2\,\underline{3}\,4)_{plate}$	[7 2 5], 71.24°	None	
550 °C/1 h	(3 1 8)	$(1\,1\,1)_{powder}\|(3\,\underline{1}\,2)_{plate}$	[3 1 4], 51.89°	⟨1 1 0⟩ 70.53° Σ = 3	3.68° < 8.66°
550 °C/1 h	(3 1 8)	$(1\,1\,1)_{powder}\|(4\,\underline{1}\,3)_{plate}$	[4 1 5], 47.21°	None	
550 °C/1 h	(3 1 8)	$(1\,1\,1)_{powder}\|(3\,\underline{2}\,1)_{plate}$	[3 2 5], 72.02°	None	
550 °C/1 h	(3 1 8)	$(1\,1\,1)_{powder}\|(0\,1\,0)_{plate}$	[1 0 1], 54.74°	None	
550 °C/8 h	(1 1 2)	$(1\,1\,1)_{powder}\|(\underline{3}\,5\,4)_{plate}$	[1 7 8], 60.67°	None	
550 °C/8 h	(1 1 2)	$(1\,1\,1)_{powder}\|(4\,0\,3)_{plate}$	[3 1 4], 36.07°	⟨4 3 1⟩ 137.17° Σ = 15	0.48° < 3.87°
550 °C/8 h	(1 1 2)	$(1\,1\,1)_{powder}\|(7\,1\,\underline{1})_{plate}$	[1 4 3], 43.31°	None	
600 °C/0.5 h	(4 3 9)	$(1\,1\,1)_{powder}\|(\underline{2}\,8\,1)_{plate}$	[7 3 10], 60.89°	None	
600 °C/0.5 h	(4 3 9)	$(1\,1\,1)_{powder}\|(0\,2\,1)_{plate}$	[1 1 2], 39.23°	⟨1 1 2⟩ 135.58° Σ = 7	5.19° < 5.67°
600 °C/0.5 h	(4 3 9)	$(1\,1\,1)_{powder}\|(1\,4\,7)_{plate}$	[1 2 1], 31.48°	None	
600 °C/0.5 h	(4 3 9)	$(1\,1\,1)_{powder}\|(\underline{4}\,1\,6)_{plate}$	[1 2 1], 76.24°	⟨1 1 2⟩ 78.46° Σ = 15	2.22° < 3.87°
600 °C/0.5 h	(4 3 9)	$(1\,1\,1)_{powder}\|(\underline{2}\,\underline{1}\,8)_{plate}$	[9 10 1], 69.66°	⟨1 1 0⟩ 70.53° Σ = 3	5.87° < 8.66
600 °C/0.5 h	(4 3 9)	$(1\,1\,1)_{powder}\|(0\,\underline{1}\,4)_{plate}$	[5 4 1], 65.16°	None	
600 °C/0.5 h	(4 3 9)	$(1\,1\,1)_{powder}\|(\underline{1}\,\underline{3}\,3)_{plate}$	[3 2 1], 97.61°	⟨3 2 1⟩ 86.18° Σ = 15	3.77° < 3.87
600 °C/0.5 h	(4 3 9)	$(1\,1\,1)_{powder}\|(1\,\underline{4}\,3)_{plate}$	[7 2 5], 69.66°	None	
600 °C/0.5 h	(4 3 9)	$(1\,1\,1)_{powder}\|(\underline{4}\,\underline{6}\,3)_{plate}$	[1 1 9 2], 109.21°	⟨1 1 0⟩ 109.47 Σ = 3	
600 °C/1.0 h	(4 1 6)	$(1\,1\,1)_{powder}\|(\text{——})_{plate}$	[40 27 13], 56.25°	⟨3 2 1⟩° Σ = 9	
700 °C/0.5 h	(1 3 4)	$(1\,1\,1)_{powder}\|(1\,8\,6)_{plate}$	[2 5 7], 30.49°	None	
700 °C/0.5 h	(1 3 4)	$(1\,1\,1)_{powder}\|(7\,4\,1)_{plate}$	[1 2 1], 31.48°	None	
700 °C/0.5 h	(1 3 4)	$(1\,1\,1)_{powder}\|(4\,1\,1)_{plate}$	[0 1 1], 35.26°	⟨1 1 0⟩ 38.94° Σ = 9	3.68° < 5.00°
700 °C/0.5 h	(1 3 4)	$(1\,1\,1)_{powder}\|(7\,\underline{1}\,1)_{plate}$	[0 1 1], 66.16°	⟨1 1 0⟩ 70.53° Σ = 3	4.37° < 8.66°
700 °C/0.5 h	(1 3 4)	$(1\,1\,1)_{powder}\|(8\,\underline{3}\,2)_{plate}$	[1 10 11], 78.62°	None	
700 °C/0.5 h	(1 3 4)	$(1\,1\,1)_{powder}\|(7\,\underline{6}\,2)_{plate}$	[8 5 13], 79.42°	None	
700 °C/0.5 h	(1 3 4)	$(1\,1\,1)_{powder}\|(\underline{1}\,\underline{1}\,4)_{plate}$	[1 1 0], 74.21°	⟨1 1 0⟩ 70.53° Σ = 3	3.68° < 8.66°
700 °C/0.5 h + 475 °C/48 h	(1 3 4)	$(1\,1\,1)_{powder}\|(5\,\underline{1}\,1)_{plate}$	[1 2 3], 56.25°	⟨3 2 1⟩ 123.75° Σ = 9	0.00°
700 °C/0.5 h + 475 °C/48 h	(1 3 4)	$(1\,1\,1)_{powder}\|(8\,1\,1)_{plate}$	[0 1 1], 44.71°	None	
700 °C/0.5 h + 475 °C/48 h	(1 3 4)	$(1\,1\,1)_{powder}\|(3\,7\,\underline{2})_{plate}$	[9 5 4], 54.08°	None	
700 °C/0.5 h + 475 °C/48 h	(1 3 4)	$(1\,1\,1)_{powder}\|(1\,5\,1)_{plate}$	[10 1], 38.94°	⟨1 1 0⟩ 38.94° Σ = 9	0.00°
700 °C/0.5 h + 475 °C/48 h	(1 3 4)	$(1\,1\,1)_{powder}\|(7\,8\,6)_{plate}$	[21 1], 6.65°	low angle	6.65 < 15°
700 °C/0.5 h + 475 °C/48 h	(1 3 4)	$(1\,1\,1)_{powder}\|(\underline{1}\,6\,5)_{plate}$	[1 6 7], 42.84°	None	
700 °C/0.5 h + 475 °C/48 h	(1 3 4)	$(1\,1\,1)_{powder}\|(\underline{1}\,2\,4)_{plate}$	[2 5 3], 50.95°	None	
700 °C/0.5 h + 475 °C/48 h	(1 3 4)	$(1\,1\,1)_{powder}\|(1\,\underline{3}\,4)_{plate}$	[7 3 4], 76.91°	None	

shown in column six of the table. An upper-bound estimate for the deviation is given by the sum of the deviation of the rotation angle and the angular deviation of the rotation axis from the ideal rotation axis. The actual deviation from ideal orientation is smaller, because only the components of the rotation angle and axis in the plane of the special boundary contribute to the deviation. The approximate maximum deviation from ideality is given by the Brandon criterion [16].

$$\theta = \theta_0 \Sigma^{-1/2}$$

where θ is the misorientation from the special boundary orientation, θ_0 is equal to 15° and Σ is the special grain boundary number.

A comparison of the Brandon criterion with an upper-bound estimate of the deviation of the crystals from the orientation of a Σ boundary of the CSL model is shown in the last column in Table II.

For the sensitization data, of the 33 powder poles "collected" by combining the data from all five, single-temperature heat treatments, 15 are geometrically special boundaries. The remaining 18 boundaries have deviations that are too high to be considered special boundaries. Of the special orientations, five represent the twin boundary, $\Sigma = 3$; three are $\Sigma = 9$ boundaries; two are $\Sigma = 11$ boundaries; two are $\Sigma = 7$ boundaries; and three are $\Sigma = 15$ boundaries.

The low-temperature sensitization results, shown at the end of Table II, were obtained by combining the information from the sample which had been given the two-part heat treatment. Of the eight powder poles collected, three are special boundaries. One is well within the low-angle boundary limit and two are $\Sigma = 9$ boundaries.

It should be noted that some of the $\Sigma = 3$ boundaries may not correspond to boundaries between the plate and powder particles but to possible twin boundaries in the austenite baseplate. If the area of a twinned region in the baseplate collected by the X-ray beam is comparable to the area of the powder, their diffracted spots would have equivalent intensities and there would be no way to distinguish between these two possibilities on the pole figure.

There are several results of the orientation measurements that are worth emphasizing. First, in all of the results, there is only one boundary that corresponds to a low angle boundary, a surprising result since the resistance to sensitization of low-angle boundaries is well documented [7, 17]. One explanation is that this is a byproduct of the X-ray technique. The pole figure method used here can only resolve poles at least 5° apart. Therefore, it is possible that remaining low-angle orientations could not be distinguished from the baseplate orientations in the pole figures. Another possibility is that very few low angle boundaries existed among the ≈ 1000 grain boundaries originally formed. This is possible since the "powder" consisted of individual, faceted grains that were once part of a polycrystalline sample and hence, unlike spheres, were unable to quickly rotate into low energy orientations with respect to the baseplate. This result confirms the ability of this sintering technique to create a large variety of grain boundary orientations.

Another interesting result is that the $\Sigma = 9$ boundary is found in the plurality in both the isothermally and low temperature sensitized samples. It is safe to say that this boundary is resistant to sensitization in austenitic stainless steels. Third, many of the boundaries observed to be unsensitized were not boundaries that were specified as special by the CSL grain boundary model. Fourth, to the extent that inferences can be drawn from the results on a small number of resistant grains, there seems to be no significant difference in the percentage of special boundaries between the single temperature sensitization and the two-temperature sensitization treatments. Finally, the orientation of the sintered surface of the single crystal baseplate may have an effect on sensitization. Each of these four results is discussed in order below.

The $\Sigma = 9$ grain boundary was analysed in a TEM study performed by Clark and Smith [18] in 1979. The study was not of sensitization, but of grain boundary dislocation interactions during high temperature grain boundary migration. The $\Sigma = 9$ boundary can be formed by a 38.94° rotation about the $\langle 1\,1\,0 \rangle$ axis. It was found that the structure of the $\Sigma = 9$ boundary allows for efficient migration of dislocations through the boundary, and so boundary migration is fast. This has important implications for the sensitization resistance of stainless steels, because this migration can introduce asymmetries in the chromium depletion profiles perpendicular to the direction of grain boundary motion [2, 19]. The formation of asymmetric chromium depleted zones does not explain the sensitization resistance of $\Sigma = 9$ boundaries. However, enhanced mobility suggests that if carbides do precipitate on $\Sigma = 9$ boundaries, then their resistance to sensitization might result from the migration of the grain boundaries away from the carbides and the chromium depleted zones. In addition, Sutton and Vitek [20] have calculated that the $\Sigma = 9$ (1 1 4) boundary in aluminium consists of alternating units of A and B, where A is the structural repeat unit that comprises the $\Sigma = 11$ (1 1 3) boundary and B is the structural unit that composes the $\Sigma = 27$ (1 1 5) grain boundary. The ABABAB... structure of the $\Sigma = 9$ boundary does not generate long range stress fields. The absence of the long range stress fields may also contribute to the sensitization resistance of the $\Sigma = 9$ grain boundaries. Liu *et al.* [6] confirm this preference for the $\Sigma = 3$ and $\Sigma = 9$ boundaries to be resistant to carbide precipitation in a ternary nickel alloy, but also include the $\Sigma = 27$ boundary, another multiple twin boundary (Σ^{3n}, $n = 2, 3, \ldots$).

The results in Table II indicate that of the 58 boundaries judged to have good resistance to sensitization, 24 or 41% exhibited values of Σ that were less than or equal to 19. Of these eight had $\Sigma = 3$, seven had $\Sigma = 9$ and one possessed a low angle grain boundary. Excluding these 16 special boundaries from consideration, then there were a total of 42 high angle boundaries that were resistant to sensitization and eight or 19%, of these had $5 \leq \Sigma \leq 19$ (excluding $\Sigma = 9$). Consequently, the CSL model is not very effective in identifying boundaries resistant to sensitization. Two studies, one by Ortner and Randle [7] in

1989, and the other by Laws and Goodhew [8] in 1991, sought to relate the extent of sensitization in austenitic stainless steel with a geometric description of the grain boundary. Ortner and Randle studied the sensitization resistance of 89 boundaries, 24 had $\Sigma = 1$, 3 or 9. Excluding these from consideration, 6 out of 10 or 60% of boundaries with $\Sigma \leq 33$ were completely or partially resistant to sensitization. Only 15 out of 41 or 36.6% general grain boundaries were completely or partially resistant to sensitization. Thus Ortner and Randle found a greater resistance of boundaries with low Σ to sensitization than was found in the present study. However, Ortner and Randle concluded that the CSL model was not very effective in judging resistance to sensitization since in several instances they noted that the intergranular corrosion attack of the boundary changed simply because the plane of the grain boundary changed while the value of Σ remained unchanged. Thus, as noted by Ortner and Randle, the categorization of boundaries into low angle, twin and high angle grain boundaries is as effective as one based on the CSL model [7].

The study by Laws and Goodhew [8] used an electron probe to measure the full-width-half-maximum (FWHM) of the chromium depletion profile around stainless steel grain boundaries. They reported that the boundaries with the narrowest chromium depleted zones exhibited Σ values of 3, 13 and 11. However, the width of the chromium depleted zone of a boundary with $\Sigma = 9$ was more than twice as great as the widths of the zones for the boundaries with $\Sigma = 3$ and 13. Furthermore, many general grain boundaries had widths that were much smaller than that of the $\Sigma = 9$ boundary. This is yet one more illustration of the fact that not all boundaries with low values of Σ have special properties. It is possible that the wide width of the depleted zone of the $\Sigma = 9$ boundary is the result of its high mobility. If so, the high mobility of the $\Sigma = 9$ boundary could reconcile the otherwise contradictory results of Laws and Goodhew, who found wide chromium-depleted zones along a $\Sigma = 9$ boundary, and the results in the present study and of Ortner and Randle [7], which found $\Sigma = 9$ grain boundaries to have superior resistance to sensitization. Laws and Goodhew did conclude that the grain misorientation across the grain boundary had little effect on the width of the chromium depleted zone. Instead they suggested that the atomic structure at the boundary, which influenced the extent and magnitude of stress fields within the grains directly influenced the widths of the chromium depleted zones.

To compare these results directly with studies that measure the chemical profile across boundaries, we must consider the fact that in this case we have begun with an asymmetric carbon concentration profile. Recall that during processing of the small austenite powder, material is given a severe sensitization treatment, and it is possible that the carbon concentration remaining in the separated grains can be as low as the solubility limit. This should have at most a minimal effect on the sensitization results for the following reasons: first, the rate-limiting step for carbide precipitation is diffusion of chromium, not carbon; second, although the carbon concentration does affect the activity, and therefore diffusion, of chromium, it will most likely be a small effect, given the small amount of carbon present to begin with [21], finally, the carbon-depleted grains are small in comparison with the austenite baseplate, which can be thought of as an infinite source of 0.06% carbon to supply carbide growth.

Intergranular precipitation may be subdivided into two steps: nucleation and growth. The initial temperature treatment of the two-step sensitization process is thought to enhance nucleation, so nucleation is not likely to be the rate limiting reaction. The overall sensitization behaviour of the material is thought to be dictated by the growth of the chromium-depleted zones at the lower, second temperature. This is suggested by the fact that only $\approx 50\%$ of the grain boundaries were sensitized by heat treatment at 700 °C/0.5 h and $\approx 90\%$ of the boundaries were sensitized by the two-step treatment of 700 °C/0.5 h + 475 °C/24 h. The data show no large differences between the results of the low temperature and the normal sensitization treatments, suggesting that grain misorientation primarily affects the carbide growth process in both single-temperature and two-temperature sensitization treatments. Presumably the rate limiting step in the growth of intergranular carbides is the transport of chromium to the precipitate, which may be enhanced by the stress field [22] of the grain boundary. Long range stress fields are absent for boundaries composed of single structural units and also boundaries composed of multiple structural units with a very short period. This may account for the sensitization resistance of some low Σ boundaries (e.g. $\Sigma = 9$ and 11 boundaries), and the sensitization susceptibility of general, high angle boundaries. As previously mentioned, it is not possible to generate explanations based on grain misorientation to account for the sensitization resistance of the many high angle boundaries present in Table II, especially given the small number of resistant grains collected. However, the presence of particular grain boundary structures that minimize long range stress fields may play a determining role.

Finally, it is noteworthy that four out of the seven baseplate orientations used in this present study are clustered near two major planes: the $\langle 3\,1\,8 \rangle$ and $\langle 4\,3\,9 \rangle$ poles are close to the $\langle 1\,1\,2 \rangle$ poles, and $\langle 8\,1\,8 \rangle$ pole is close to the $\langle 0\,1\,1 \rangle$ pole. This may be a consequence of texturing during the thermomechanical processing of the austenite baseplates. Very few of the grains sintered to the baseplates with the $\{8\,1\,8\}$ orientation remained attached to the baseplate after the sensitizing treatment and the ASTM A262E test. That is, most of the boundaries were sensitized, yet two out of three of the unsensitized grain boundaries are special boundaries. Conversely, for the $\{4\,3\,9\}$ an $\{3\,1\,8\}$ baseplates, many more of the boundaries were left unsensitized, but a smaller proportion of those boundaries are geometric special boundaries.

Electron microscopy has demonstrated that the preferred interface between carbide precipitates and stainless steel matrix is that of $\{1\,1\,1\}_{M_{23}C_6} \| \{1\,1\,1\}_{Steel}$ [23–25]. Typically, the carbide nucleus which forms on a grain boundary shares the preferred orientation

with one of the grains forming the grain boundary. Growth of the carbide then occurs into the other grains [24]. There is good atomic matching between the carbide and matrix across $\{1\,1\,1\}$ in $\langle 1\,1\,0\rangle$ in both lattices, implying that grains with $\langle 1\,1\,0\rangle$ in the plane of the boundary will provide favourable carbide nucleation sites. Both sets of baseplates, those nearly parallel to $\{1\,1\,2\}$ and the others nearly parallel to $\{1\,1\,0\}$ contain $\langle 1\,1\,0\rangle$ and should therefore be suitably oriented for carbide nucleation. However, the much greater incidence of sensitization of grains sintered to baseplates nearly parallel to $\{1\,1\,0\}$ compared to baseplates nearly parallel to $\{1\,1\,2\}$ suggests that there may be additional crystallographic and/or structural effects that influence intergranular carbide precipitation. Grain boundary ledges and dislocations, for example, are thought to promote the nucleation of $M_{23}C_6$ [25]. Whatever the nature of the elements of grain boundary structure that promote carbide precipitation it is clear that a much greater number exist in boundaries nearly parallel to the $\{1\,1\,0\}$ in one grain than in boundaries nearly parallel to the $\{1\,1\,2\}$ of one grain.

5. Summary

In a study of approximately 1000 individual grains, which were sintered to single crystals, only 5% were resistant to sensitization. X-ray analyses of the orientations of the individual grains and single crystals indicate that macroscopic grain boundary geometry cannot explain the sensitization behaviour of most grain boundaries. Nevertheless, the $\Sigma = 9$ boundary was found to be resistant to sensitization. Comparing the boundaries resistant to single-temperature sensitization treatments to the boundaries resistant to two-temperature sensitization treatments suggests that grain misorientation primarily influences growth of sensitization, rather than nucleation. Finally, the crystallographic plane of the grain boundary appears to have an effect on sensitization.

Acknowledgements

The authors wish to thank Professor Rudy Wenk for many helpful discussions and assistance with the X-ray measurements.

References

1. C. L. BRIANT and E. L. HALL, *Corrosion* **42,** (1986) 9.
2. E. L. HALL and C. L. BRIANT, *Met. Trans. A* **154**, (1984) 793.
3. R. A. MULFORD, E. L. HALL and C. L. BRIANT, *Corrosion* **39**, (1982) 4.
4. K. L. MERKLE and D. WOLF, *MRS Bull.* **15**, (1990) 42.
5. M. L. KRONBERG and F. H. WILSON, *Trans. Amer. Inst. Min. Engng.* **215**, (1959) 820.
6. H. LIU, M. GAO, D. G. HARLOW and R. P. WEI, *Scripta Metall.* **32**, (1995) 1807.
7. S. R. ORTNER and V. RANDLE, *ibid.* **23**, (1989) 1903.
8. M. S. LAWS and P. J. GOODHEW, *Acta Metall. Mater.* **39**, (1991) 1525.
9. G. H. BISHOP and B. CHALMERS, *Scripta Metall.* **2**, (1968) 133.
10. P. G. SHEWMON, "Recrystallization, Grain Growth and Textures" (American Society for Materials, Metals Park, Ohio, 1966) p. 165.
11. G. HERRMANN, H. GLEITER and G. BARO, *Acta Metall.* **24**, (1976) 353.
12. American Society for Testing and Materials, ASTM Specification A262E-70 (ASTM, Philadelphia, PA).
13. A. KAVNER, MS thesis, Department of Materials Science and Mineral Engineering, University of California, Berkeley, USA (1992).
14. C. STAWSTROM and M. HILLERT, *J. Iron Steel Inst.* **207**, (1969) 77.
15. C. S. TEDMON, D. A. VERMILYEA and J. H. ROSOLOWSKI, *J. Electrochem. Soc.* **118**, (1971) 192.
16. D. G. BRANDON, *Acta Metall.* **14**, (1966) 1470.
17. B. W. BENNETT and H. W. PICKERING, *Met. Trans. A.* **18A**, (1987) 1117.
18. W. A. T. CLARK and D. A. SMITH, *J. Mater. Sci.* **14**, (1979) 776.
19. T. A. MOZHI, H. S. BETRABET, V. JAGANNATHAN, B. E. WILDE, and W. A. T. CLARK, *Scripta Metall.* **20**, (1986) 723.
20. A. P. SUTTON and V. VITEK, *ibid.* **14**, (1980) 129.
21. C. S. TEDMON, D. A. VERMILYEA and J. H. ROSOLOWSKI, *J. Electrochem. Soc.* **118**, (1971) 192.
22. P. G. SHEWMON, "Diffusion in Solids", (McGraw Hill, NY, 1963).
23. M. H. LEWIS and B. HATTERSLEY, *Acta Metall.* **13**, (1965) 1159.
24. L. K. SINGHAL and J. W. MARTIN, *Trans. Metall. Soc. AIME* **242**, (1968) 814.
25. J. P. ADAMSON and J. W. MARTIN, *Acta Metall.* **19**, (1971) 1015.

Received 31 October 1995
and accepted 17 September 1996